

## Interplay of Conductance, Force, and Structural Change in Metallic Point Contacts

Markus Ternes,<sup>1,2,\*</sup> César González,<sup>3,4</sup> Christopher P. Lutz,<sup>1</sup> Prokop Hapala,<sup>3</sup>  
Franz J. Giessibl,<sup>5</sup> Pavel Jelínek,<sup>3,†</sup> and Andreas J. Heinrich<sup>1</sup>

<sup>1</sup>IBM Research Division, Almaden Research Center, 650 Harry Road, San Jose, California 95120, USA

<sup>2</sup>Max-Planck-Institut für Festkörperforschung, D-70569 Stuttgart, Germany

<sup>3</sup>Institute of Physics, Academy of Sciences of the Czech Republic, Cukrovarnicka 10, 162 00, Prague, Czech Republic

<sup>4</sup>Instituto Ciencia de Materiales de Madrid, 28049 Cantoblanco, Madrid, Spain

<sup>5</sup>Institute of Experimental and Applied Physics, University of Regensburg, D-93053 Regensburg, Germany

(Received 31 August 2010; published 5 January 2011)

The coupling between two atomically sharp nanocontacts provides tunable access to a fundamental underlying interaction: the formation of the bond between two atoms as they are brought into contact. Here we report a detailed experimental and theoretical analysis of the relation between the chemical force and the tunneling current during bond formation in atom-scale metallic junctions and their dependence on distance, junction structure, and material. We found that the short-range force as well as the conductance in two prototypical metal junctions depend exponentially on the distance and that they have essentially the same exponents. In the transition regime between tunneling and point contact, large short-range forces generate structural relaxations which are concomitant with modifications of the surface electronic structure and the collapse of the tunneling barrier.

DOI: 10.1103/PhysRevLett.106.016802

PACS numbers: 73.22.-f, 73.63.Rt, 74.55.+v

While the first simultaneous measurements of the distance dependency of force and conductance were already performed a decade ago [1–3], the question of how the short-range forces relate to the tunneling conductance is still in theoretical and experimental debate [4–6]. Recently, these quantities have been precisely determined in a single measurement by using a combined scanning tunneling (STM) and atomic force microscope [7,8]. Such an instrument allows one to measure simultaneously the conductance and the short-range force between an atomically sharp tip and well characterized adsorbates on surfaces.

In this Letter, we present measurements and simulations of prototypical atomic junctions between an individual metal adsorbate on a metal substrate and a metallic tip [Fig. 1(a)]. All experiments were performed in ultrahigh vacuum ( $p < 10^{-8}$  Pa) and at a temperature of about 5 K [9]. To discriminate between the short-range force which originates from the direct interaction of the adsorbate and the tip apex and all long-range forces between the macroscopic sample and tip, we measure directly on top of the adsorbate and again at a lateral distance of  $\approx 1.5$  nm. At this distance the force is no longer influenced by the adsorbate and only long-range forces contribute to the frequency shift  $\Delta f$  of the force-sensing cantilever which oscillates normal to the surface (for details of the setup, see [9]). In Fig. 1(b) we show the  $\Delta f$  data measured on top and off a single Pt atom adsorbed on a clean Pt(111) surface at different tip-sample distances  $d$  and the corresponding time-averaged conductance  $G_{\text{av}}$  (the conductance averaged over the oscillation of the cantilever) and dissipation  $D$ . We used the  $\Delta f$  data to calculate the short-range force normal to the surface  $F_z = F_{\text{on}} - F_{\text{off}}$  using the Sader-Jarvis

formalism [10] [Fig. 1(c)] and the  $G_{\text{av}}$  data to calculate the instantaneous conductance  $G$  by removing the smearing induced by the tip oscillation [11] [Fig. 1(d)].

We observe at  $d \approx 0$  the minimum of  $F_z = -1.9$  nN concomitant with a conductance of  $G \approx G_0$ . For smaller tip-sample distances the force increases until force equilibrium at  $d = -0.5$  Å is reached. We note that the forming and breaking of this chemical bond does not significantly increase the intrinsic dissipation  $D$  of the cantilever which varies only between 1–3 meV per oscillation cycle, which is very small compared to the total bonding energy of  $\approx 1$  eV [Fig. 1(b)] [9].

The small  $D$  and unchanged STM images taken before and after bond forming suggest that the tip apex and the adsorbate-sample system stay unaltered and only deform elastically.

We performed similar experiments on individual Cu adatoms on a Cu(111) surface [Fig. 2(b) and [9]]. The maximal attraction is smaller than on the Pt/Pt(111) system and reaches only  $-0.8$  nN at  $d \approx 0.25$  Å. At this tip-sample distance the conductance is close to  $0.75 G_0$  while for smaller  $d$  it increases to approximately  $G_0$ .

For both systems we found that in the tunneling regime ( $d \geq 0.75$  Å)  $G$  as well as  $F_z$  change exponentially as the tip approaches the adsorbate (Fig. 2), i.e.,

$$F_z(d) \propto \exp(-d/\lambda_F) \quad \text{and} \quad G(d) \propto \exp(-d/\lambda_G), \quad (1)$$

with  $\lambda_F$  and  $\lambda_G$  as the characteristic decay length of the short-range force and the conductance, respectively. The exponential decay stems from the fact that both  $F_z$  and  $G$  depend on the orbital overlap of the wave functions of tip and sample.

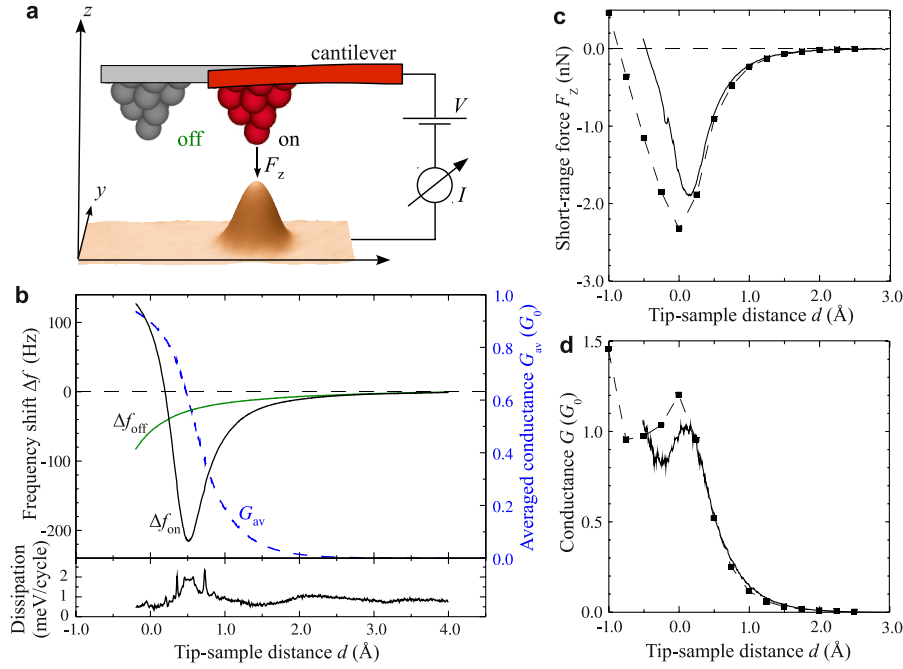


FIG. 1 (color online). (a) 3D representation of a constant current STM image ( $I = 1$  nA,  $V = 1$  mV,  $4 \times 1.5$  nm<sup>2</sup>) of a single Pt atom adsorbed on a Pt(111) surface and a schematic of the probing tip. (b) Time-average junction conductance  $G_{av} = I_{av}/V$  (blue dashed curve) and frequency shift  $\Delta f$  on top (black curve) and off (green curve) the Pt atom measured at different tip-sample distances  $d$ . The lower panel shows the dissipation signal  $D$  on top of the Pt atom recorded simultaneously with  $G_{av}$  and  $\Delta f$ . (c) Calculated short-range force between tip apex and Pt adatom (full line) and simulated forces (squares) from data in (b). (d) Conductance after deconvolution of the tip oscillation (full line) and simulated conductance (squares). All conductances are given in units of the single-channel, spin-degenerate quantum of conductance  $G_0 = 2e^2/h = (12906 \Omega)^{-1}$ , where  $e$  is the elementary charge and  $h$  is the Planck constant.

In contrast to the uniform exponential change and the smooth transition to the maximal absolute value of  $G$  in the Pt/Pt(111) system [Fig. 2(a)], the Cu/Cu(111) system shows an overshooting, i.e., a decrease of  $\lambda_G$ , at the transition

between tunneling and point contact ( $0 < d < 0.75$   $\text{\AA}$ ) [Fig. 2(b)]. While this decrease of  $\lambda_G$  close to point contact was already observed in STM only measurements [12], here we can relate it to the simultaneously measured divergence of the exponential  $F_z$  dependence which is even stronger in the Pt/Pt(111) system than in the Cu/Cu(111) system.

To explain the measurements, extensive total energy density functional calculations using the VASP code [13] in combination with a Green's function approach [14] for the electron transport were performed (for details, see [9]). We note that this simulation takes all atomic and electronic relaxation of tip and sample into account and allows a nonperturbative treatment of the electron transport in both the tunneling and contact regimes.

First, we performed an extensive search for a reliable tip structure. Different tip geometries have been explored and compared with the experimental  $F_z$  and  $G$  curves whereby a regularly pyramidal Ir tip with a (100) [for the Pt/Pt(111) system] or (111) [for the Cu/Cu(111) system] fcc surface facet and terminated at the apex with an atom of the surface material (Pt or Cu, respectively) shows the best conformance with the experimental data of both systems [9]. In both systems we find very good agreement between experimental and calculated data as shown in Figs. 1 and 2. In addition, we observe in our simulations a strong dependence of the force on the chemical composition of the outermost tip atom indicating a possible single-atom chemical identification [15].

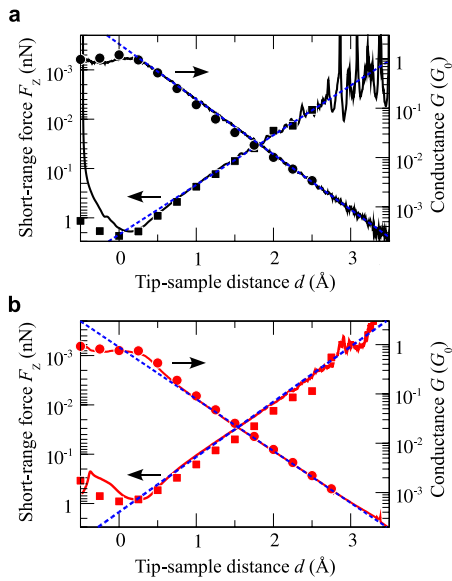


FIG. 2 (color online). (a) Logarithmic plot of the conductance  $G$  and short-range force  $F_z$  as measured (full line) and simulated (dots and squares) for the Pt/Pt(111) system. (b) Same as (a) but for Cu/Cu(111). Blue dashed lines in both panels are exponential fits for  $d \geq 0.75$   $\text{\AA}$  to the  $G$  and  $F_z$  data, respectively.

In the tunneling regime the exponents  $\lambda_F^{-1}$  and  $\lambda_G^{-1}$  of the experimental and simulated data are very close to each other and their ratio  $\alpha = \lambda_G/\lambda_F$  for both systems is  $\approx 1$  (see Table I). Thus, in this distance range of an atomic metal junction, force and conductance are proportional to each other ( $F_z \propto G$ ). The decay coefficient of the conductance  $\kappa = \frac{1}{2}\lambda_G^{-1}$  is related to the apparent tunneling barrier height  $\Phi$  between tip and sample as  $\kappa = \sqrt{2m\Phi}/\hbar$ , with  $m$  as the electron mass and  $\hbar$  as the reduced Planck constant [16]. We find in our experimental data an apparent barrier height of  $6.3 \pm 0.4$  eV ( $5.6 \pm 0.3$  eV) for the Pt (Cu) system, similar to earlier measurements [12,17].

While the exponential decay of the conductance is beyond controversy, different theoretical predictions have been made for the ratio  $\alpha$  between short-range force and conductance. Chen found  $\alpha = 2$  by using first-order perturbation theory for the hydrogen molecule ion [18,19], and by canonical transformation and diagonalizing the tunneling transfer Hamiltonian [17]. In contrast, Hofer and Fisher found in the framework of the scattering formalism and second-order perturbation  $\alpha = 1$  [4]. Recently, another model incorporating both regimes depending on electronic structure of an atomic contact has been introduced [20]. Here, the clear results we found experimentally and by simulation, going beyond the perturbation theory, answer the theoretical controversy [4–6,18] of the relationship between  $F_z$  and  $G$  in metallic junctions.

The simulations provide detailed insight into underlying processes during the formation of the atomic contact. In particular, we found five main correlated factors related to the formation of the chemical bond between tip and sample: (i) structural relaxation of atoms forming the contact [21–23], (ii) modification of the surface electronic structure [24,25], (iii) collapse of the tunneling barrier [26], (iv) conductance saturation via elastic multiple-scattering processes in near-to-contact regime [14], and (v) modification of surface dipole responsible for atomic contrast observed recently in a kelvin force probe microscope [27].

TABLE I. Decay coefficients  $\lambda_F^{-1}$  and  $\lambda_G^{-1}$  of the short-range force  $F_z$  and the conductance  $G$  determined by fitting the experimental and calculated data shown in Figs. 1 and 2 for tip-sample distances  $d \geq 0.75$  Å. From  $\lambda_G$  the apparent barrier height  $\Phi$  can be calculated. The ratio  $\alpha = \lambda_G/\lambda_F$  is surprisingly close to 1 for both systems. We note that the uncertainty of the experimentally determined values is mainly due to systematic errors in the determination of the tip-sample distance  $d$ , but this error does not influence the uncertainty of the experimentally observed  $\alpha$ .

	$\lambda_F^{-1}$ (Å <sup>-1</sup> )	$\lambda_G^{-1}$ (Å <sup>-1</sup> )	$\Phi$ (eV)	$\alpha = \lambda_G/\lambda_F$
Pt (exp.)	$2.42 \pm 0.08$	$2.58 \pm 0.08$	$6.3 \pm 0.4$	$0.94 \pm 0.01$
Pt (sim.)	$2.46 \pm 0.06$	$2.56 \pm 0.06$		$0.96 \pm 0.04$
Cu (exp.)	$2.64 \pm 0.08$	$2.42 \pm 0.08$	$5.6 \pm 0.3$	$1.09 \pm 0.01$
Cu (sim.)	$2.56 \pm 0.10$	$2.50 \pm 0.04$		$1.02 \pm 0.06$

Our simulations yield that both studied systems show a profound structural change at the transition between tunneling and point contact [23,28]. The topmost atom of the tip apex and the adsorbate move towards each other with increasing attractive force  $F_z$ . Figure 3 shows that for the Cu adsorbate on the Cu(111) the relaxation is almost as large ( $\Delta d_S = 0.6$  Å) as for the Pt adsorbate on the Pt(111) surface ( $\Delta d_S = 0.7$  Å) even though the maximal attractive force differs between both systems by a factor of  $\approx 2.6$  in the simulation and  $\approx 2.2$  in the experiment. This is in contrast to the deformation in the tip apex, which is approximately proportional to  $F_z$ . We attribute this behavior to the different Young's modulus of the two materials which is with  $Y = 120$  GPa for Cu much lower than  $Y = 168$  GPa for Pt [29]. Between  $d = 0.25$  Å and  $d = 0$  the calculations show a large (0.3–0.5 Å) change in the relaxation between tip and sample (Fig. 3). This resembles snap to contact as it was found, for example, in experiments on Au adatoms on Au(111) [23]. However, the negligible dissipation signal [Fig. 1(b)] indicates that snap to contact does not play a role in our experiments.

Furthermore, we found in the junction significant modification of the surface electronic structure. The Hartree potential  $V^H$  across the junction yields the collapse of the tunneling barrier [Fig. 4(a)] [26], which is accompanied by a charge accumulation of up to 0.24 (0.15) electron charges in the Pt/Pt(111) [Cu/Cu(111)] junction [Fig. 4(b)]. This charge enhancement during the bond formation and the elastic deformation of tip and sample significantly influences the orientation and energy of the atomic orbitals which are involved in the electronic transport and the acting short-range forces [24,25]. Calculating the density of states (DOS) of the substrate-adsorbate system at the apex atom

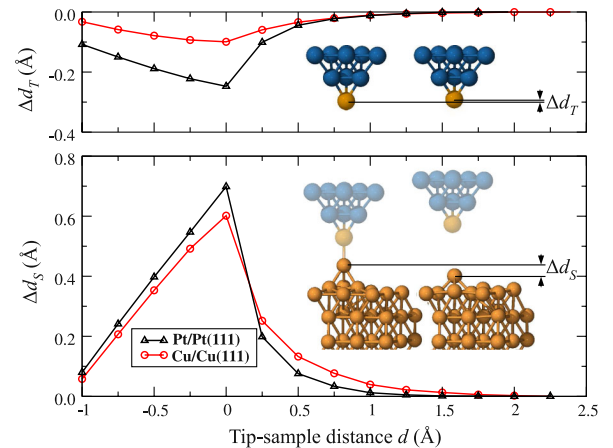


FIG. 3 (color online). Relaxations of the tip apex atom towards the surface (top) and of the surface adatom towards the tip (bottom) from the unperturbed, i.e., force-free, positions at large tip-sample distances. Black triangles (red circles) represent calculations for the Pt/Pt(111) [Cu/Cu(111)] adsorbate-sample system. Solid lines are guides to the eyes. The insets show stick-and-ball models of the Ir tip and Cu surface atoms at close ( $d = 0$ ) and at large distance ( $d = 6$  Å).

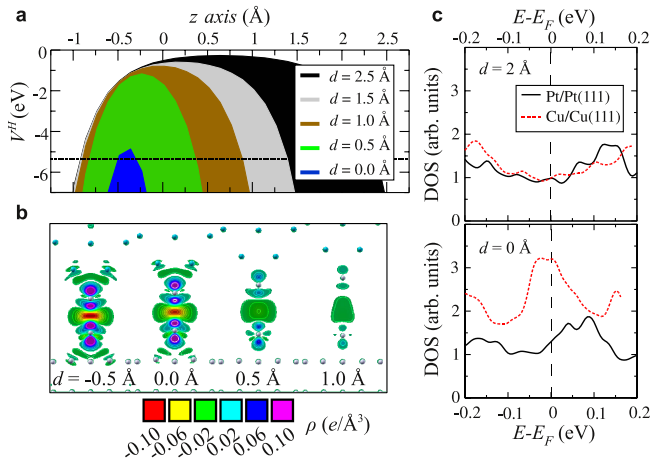


FIG. 4 (color online). (a) Cross section of the Hartree potential  $V^H$  along the  $z$  axis at different tip-sample distances  $d$  for the Pt/Pt(111) system. The dashed line marks  $E_F$  of the sample. (b) 2D cut through the junction showing the charge transfer  $\rho$  in tip and sample for different  $d$  in the Pt/Pt(111) system. Small balls mark the nuclear positions of the atoms. (c) Density of states (DOS) calculation of the substrate-adsorbate system at a tip-sample distance where  $F_z$  is maximal ( $d = 0$ ) and at  $d = 2$  Å.

of the tip reveals that the DOS around the Fermi energy  $E_F$  changes by more than a factor of 2 in the Cu/Cu(111) system when the tip approaches the point of maximal attractive force ( $d = 0$ ) while it changes only insignificantly in the Pt/Pt(111) system [Fig. 4(c)]. This increase in the DOS is mainly due to a spatial rearrangement of the  $s$  and  $d$  orbitals of the Cu adsorbate and a concomitant shift of their energy towards  $E_F$ . The higher DOS increases the probability for electrons to tunnel between tip and adsorbate and is the origin of the observed growth of  $\kappa_G$  as displayed in Fig. 2(b). Here we note that only states close to  $E_F$  contribute to the conductance, and thus the small shift of the energetic position observed in the Pt/Pt(111) system does not significantly alter the exponential behavior of  $G$ . In contrast, the growth of  $\kappa_F$  in both systems is due to structural deformations (Fig. 3) which are stronger in the Pt/Pt(111) system.

To summarize, our experimental and theoretical work offers a novel way to characterize materials on the atomic and molecular scale using the two complementary channels: force and conductance. To thoroughly understand the bond formation in nanoscale contacts a thorough interpretation of the force and conductance is necessary. As we have shown, the complex interplay between deformations and the electronic states in tip and sample and the mechanical forces and electrical conductance can be tackled by state-of-the-art calculations and verified experimentally.

We thank B. J. Melior for expert technical assistance. We acknowledge financial support from the Office of Naval Research (M. T., C. P. L., and A. J. H.), from the Spanish

Ministry of Science and Innovation (C. G.) No. MAT-2008-01497/NAN and No. CSD2007-00041, from the GAAV No. 202/09/0545 and GAAV No. M100100904 (P. P. and P. J.), and the German Federal Ministry of Education and Research (F. J. G.).

\*m.ternes@fkf.mpg.de

†jelinekp@fzu.cz

- [1] A. Schirmeisen, G. Cross, A. Stalder, P. Grutter, and U. Durig, *New J. Phys.* **2**, 29 (2000).
- [2] G. Rubio-Bollinger, P. Joyez, and N. Agrait, *Phys. Rev. Lett.* **93**, 116803 (2004).
- [3] Y. Sun *et al.*, *Phys. Rev. B* **71**, 193407 (2005).
- [4] W. A. Hofer and A. J. Fisher, *Phys. Rev. Lett.* **91**, 036803 (2003).
- [5] C. J. Chen, *Phys. Rev. Lett.* **96**, 069701 (2006).
- [6] W. A. Hofer and A. J. Fisher, *Phys. Rev. Lett.* **96**, 069702 (2006).
- [7] M. Ternes, C. P. Lutz, C. F. Hirjibehedin, F. J. Giessibl, and A. J. Heinrich, *Science* **319**, 1066 (2008).
- [8] D. Sawada, Y. Sugimoto, K. Morita, M. Abe, and S. Morita, *Appl. Phys. Lett.* **94**, 173117 (2009).
- [9] See supplementary material at <http://link.aps.org/supplemental/10.1103/PhysRevLett.106.016802> for details about the methods used.
- [10] J. E. Sader and S. P. Jarvis, *Appl. Phys. Lett.* **84**, 1801 (2004).
- [11] F. J. Giessibl and H. Bielefeldt, *Phys. Rev. B* **61**, 9968 (2000).
- [12] L. Limot, J. Kroger, R. Berndt, A. Garcia-Lekue, and W. A. Hofer, *Phys. Rev. Lett.* **94**, 126102 (2005).
- [13] G. Kresse and J. Furthmüller, *Phys. Rev. B* **54**, 11 169 (1996).
- [14] J. M. Blanco *et al.*, *Phys. Rev. B* **70**, 085405 (2004).
- [15] Y. Sugimoto *et al.*, *Nature (London)* **446**, 64 (2007).
- [16] J. G. Simmons, *J. Appl. Phys.* **34**, 1793 (1963).
- [17] C. J. Chen, *Introduction to Scanning Tunneling Microscopy* (Oxford University Press, New York, 2008), 2nd ed.
- [18] C. J. Chen, *J. Phys. Condens. Matter* **3**, 1227 (1991).
- [19] C. J. Chen, *Nanotechnology* **16**, S27 (2005).
- [20] P. Jelínek and F. Flores, arXiv:1006.3729.
- [21] L. Olesen, M. Brandbyge, M. R. Sørensen, K. W. Jacobsen, E. Lægsgaard, I. Stensgaard, and F. Besenbacher, *Phys. Rev. Lett.* **76**, 1485 (1996).
- [22] W. A. Hofer, A. J. Fisher, R. A. Wolkow, and P. Grutter, *Phys. Rev. Lett.* **87**, 236104 (2001).
- [23] J. Kröger, H. Jensen, and R. Berndt, *New J. Phys.* **9**, 153 (2007).
- [24] N. Neel *et al.*, *Phys. Rev. Lett.* **98**, 016801 (2007).
- [25] P. Jelínek, M. Švec, P. Pou, R. Perez, and V. Chab, *Phys. Rev. Lett.* **101**, 176101 (2008).
- [26] N. D. Lang, *Phys. Rev. B* **37**, 10 395 (1988).
- [27] S. Sadewasser *et al.*, *Phys. Rev. Lett.* **103**, 266103 (2009).
- [28] L. Vitali *et al.*, *Phys. Rev. Lett.* **101**, 216802 (2008).
- [29] *Handbook of Chemistry and Physics*, edited by David R. Lide (CRC Press, Boca Raton, FL, 1999), 90th ed.